IIETA International Information and Engineering Technology Association
Advancing the World of Information and Engineering

Journal Européen des Systèmes Automatisés
Vol. 59, No. 2, February, 2026, pp. 413-419
Journal homepage: http://iieta.org/journals/jesa

Parametric Optimization and Performance Analysis of a Compact Dual-Band Split Square Loop FSS for X-Band and Ku-Band

Raghad Ghalib Alsultan[1], Firas Shawkat Hamid[2*], AbdulSattar M. Khidhir[3], Muharrem Karaaslan[4], Shamil Kh. Ramadhan[5]

[1] Department of Electrical Techniques, Polytechnic College-Mosul, Northern Technical University, Mosul 41002, Iraq
[2] Department of Network Technologies and Computer Software, Polytechnic College-Mosul, Northern Technical University, Mosul 41002, Iraq
[3] Department of Network Technologies and Computer Software, Polytechnic College-Mosul and Artificial Intelligence Research Center, Northern Technical University, Mosul 41002, Iraq
[4] Department of Electrical-Electronics Engineering, Faculty of Engineering and Natural Sciences, Iskenderun Technical University, Iskenderun 31200, Turkey
[5] Department of Medical Instrumentation Techniques, Polytechnic College-Mosul, Northern Technical University, Mosul 41002, Iraq

Corresponding Author Email: dr.firas.hamid@ntu.edu.iq

https://doi.org/10.18280/jesa.590211

Received: 27 September 2025
Revised: 17 December 2025
Accepted: 2 January 2026
Available online: 28 February 2026

Keywords:
microwave filter, Frequency Selective Surface, periodic structure, split square loop, Computer Simulation Technology microwave studio

ABSTRACT

Modern wireless communication systems require higher capacity and faster data transfer rates, presenting significant challenges in signal processing. Frequency Selective Surfaces (FSSs) offer effective solutions by providing selective transmission and reflection across multiple frequency bands. This study presents a dual-band Split Square Loop Frequency-Selective Surface (SSL-FSS) optimized for X- and Ku-band applications (8 GHz and 18 GHz). Parametric analysis of gap length (g_r), leg length (s), copper width (w), and substrate thickness (n) identifies optimal dual-band operation at s = 3 mm, w = 2 mm, g_r = 0.5 mm, and n = 0.05 mm. The design records 44% bandwidth, which is better compared with the existing FSSs in terms of compactness and angular stability.

1. INTRODUCTION

Frequency Selective Surfaces (FSSs) are filters based on the use of microwave filters to provide band-pass or band-stop behaviour in frequency space. These periodic structures are periodic structures with frequency-dependent transmission and reflection characteristics that act as filters that consist of an array of elements [1]. In microwave and millimeter-wave applications, FSSs are utilised to improve the quality of a received signal, gain and directivity. They have been designed with communication systems in a number of forms, and they include dipole, Jerusalem crosses, rings, tripods, cross dipoles, and square loops [2, 3]. There are two basic types of FSS (array of wires (dipoles) and array of slots) both generally placed on a dielectric substrate. Figure 1 is a diagram of a spatial band-stop filter comprising of resonant dipole and a spatial band pass filter comprising of slots. For clarity, except for microwave filters, a FSS's frequency response is affected by polarization and incidence angle in addition to frequency [4].

The design of FSS depends on choosing appropriate parameters, as the center frequency is affected by several factors, including polarity response, element shape, and frequency bandwidth in transmission and reflection [5]. A significant care must be taken to select the appropriate element to achieve the desired mutual polarization and bandwidth [6]. The operating range of a FSSs unit cell is determined in the resonant state and depending on the shape, size of the element, and the periodicity of the cell [7]. A common geometry for doubly infinite periodic FSSs in the x−y plane is shown in Figure 2. Their transmission and reflectivity properties are sensitive to the frequency of the electromagnetic field that incident upon them due to their periodic nature. In the vicinity of the element resonance, they usually show a significant reflection [8].

By altering the frequency periodicities along the x, y, or z axes, the frequency response can be managed. To enhance the directivity of the electrically small antenna covered by the FSS, FSS screens are occasionally utilized both above and below the sides of a diffraction grating. This creates a uniform aperture distribution of the near-field [8, 9].

FSSs analysis and design, as well as parameter calculation, are inherently multidisciplinary, necessitating awareness of antenna, electromagnetic theory, and FSS analysis and modeling disciplines. For instance, when a parameter in an FSS is changed, it may have some electromagnetic consequences and thus impact the frequency filtering [10]. Generally, FSS can be engineered utilizing transmission line theory to forecast the intended transmission attributes, and it

performs a filtering operation, as the name suggests. Hence, as shown in Figure 3, they are classified on their physical construction into [11, 12]:

- Low-pass FSS filters pass low frequencies.
- High-pass filters pass high frequencies and block low frequencies.
- Stop-band filters reject unwanted frequencies.
- Pass-band filters allow specific frequencies to pass.

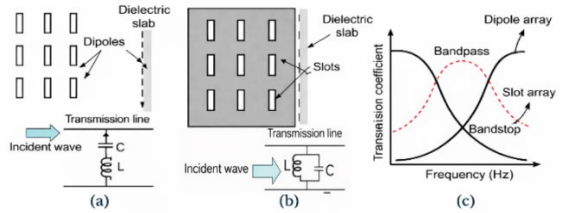

Figure 1. Basic Frequency Selective Surface (FSS) configurations: (a) dipole array, (b) slot array, and (c) frequency responses [1]

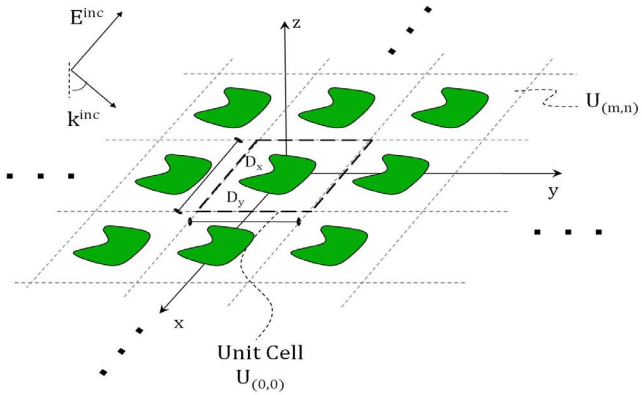

Figure 2. Regular morphology of a doubly infinite periodic Frequency Selective Surface (FSS) in the x−y plane
The element is shown by the green area. Dx and Dy denote the size of the unit cell [8]

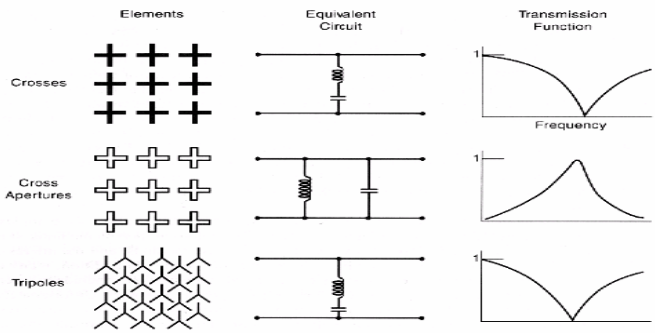

Figure 3. A Frequency Selective Surface (FSS) is adopted as a notch filter [11]

Antenna systems leverage FSSs as reconfigurable electromagnetic filters to tailor electromagnetic wave (EM) properties (frequency/polarization), benefiting from their thin profiles and manufacturability [13]. Key implementations comprise:

- Reflector antenna systems, where FSS reflectors isolate feeds operating in different frequency bands [14].
- Antenna radomes, which enhance control over transmitted and reflected waves [15].

Additional FSS applications in sixth-generation (6G) networks include interference mitigation, improved channel quality, and enhanced coverage compared to Intelligent Reflection Surfaces (IRS), with emerging use cases such as adaptive spectrum [16] as well as its use in substrate-integrated waveguide (SIW) technology, which was specifically developed for airborne radar dome applications to achieve high selectivity, low input loss, and stable angular performance [17]. Finally, electromagnetic shielding and radar cross-section reduction, where they act as slotted wideband frequency selective reflectors designed specifically for sub-6 GHz 5G devices to achieve wideband reflection performance and angular stability [18].

Modern dual-passband FSSs achieve independently tunable bands by incorporating unit cells with two distinct transmission poles [19]. A miniaturized FSS unit cell was achieved using a meandered or fractal geometry to increase the electrical length within a compact footprint [20]. This design approach ensures polarization insensitivity due to symmetrical geometry and provides angular stability because of the reduced unit cell size relative to the wavelength for Ku-band satellite communication applications. U-shaped resonator with a ground via to generate dual-band responses through multiple resonant modes. The concept relies on the U-shaped structure to provide two distinct electrical paths, enabling independent frequency tuning and polarization selectivity. As a result, the design achieves compact size, stable angular performance, and dual-band operation suitable for wireless communication applications [21], while polarization-insensitive dual-band FSSs deliver EMI shielding using compact unit cells [22]. Despite advances in optimization techniques. Recent studies indicate that dual-band FSS designs can be optimized using advanced algorithms [23]. A graphene-based reconfigurable FSS is introduced for cognitive radio applications [24]. By applying a DC bias voltage, the conductivity of the graphene layer is dynamically tuned, enabling continuous frequency shifting of the resonant response. The design achieves a tunable range of 2.1–5.2 GHz with 10–15% bandwidth and maintains polarization insensitivity and angular stability up to 50°. However, it suffers from high insertion loss and complex fabrication due to the integration of graphene with biasing networks. To address these challenges, further research is needed to optimise the fabrication process and enhance the overall efficiency of the device. Additionally, exploring alternative materials or hybrid systems could potentially reduce insertion loss while maintaining the desired performance characteristics.

This work presents a split-loop topology that supports tunable dual-band resonance at 8 GHz and 18 GHz, achieving a 44% bandwidth, as demonstrated through systematic parametric optimization.

2. RESEARCH METHODOLOGY

2.1 Filter design

In order to measure the Frequency Selective Surface (FSS) performance a loop of split squares (SSL-FSS) array is used in this study.

The dual-band resonance mechanism in frequency-selective surfaces relies on the integration of multiple resonance structures within a single cell. A parallel resonant circuit (acting as a bandpass filter) and a series resonant circuit

(acting as a bandstop filter) are combined, allowing the "transmission poles" to be tuned to pass two different frequencies. Resonance occurs when the circumference of the metallic element or aperture approaches the wavelength λ; therefore, a larger element generates a lower frequency, while a smaller element generates a higher frequency. During the design of a reconfigurable filter, a consideration of using both a parallel L-C circuit and a series L-C circuit provides more degrees of freedom compared with only one parallel or series resonance circuit. Figure 4 shows a filter with both a parallel L-C resonant circuit and a series L-C resonant circuit.

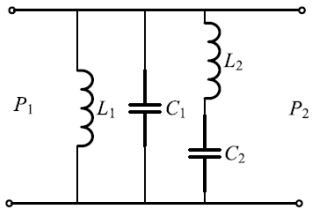

Figure 4. Filter with both a parallel L-C resonant circuit and a series L-C resonant circuit

The design parameters include element length (L), element width (w), substrate thickness (n), gap length (g_r) between the SSL sides, and leg length (s) of the SSL. Figure 5 shows the SSL-FSS geometry.

The first resonance is primarily related to the main square-loop structure, where the gap Length (g_r) affects the capacitive coupling; increasing the gap decreases the amplitude, thus raising the first resonant frequency. While the second resonance appeared when "legs" of length (s > 0) were added; these legs introduce additional inductance, creating a secondary LC resonance, (as shown in the simulation section). In brief, the transition from single to dual design was physically achieved by adding inductive and capacitive components (legs and gaps) to produce two resonant pathways within a single cell.

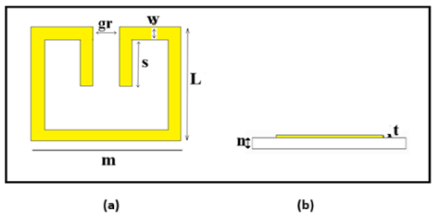

Figure 5. The Split Square Loop Frequency Selective Surface (FSS) array unit cell. (a) Top view, (b) Side view

2.2 Split Square Loop Frequency-Selective Surface unit cell design configurations

Table 1. Square loop Frequency Selective Surface (FSS) simulation parameters

Parameter	Value(mm)	Definition
M	10	unit cell size
Gr	0.5	Length of gap between the SSL sides
L	9	SSL length
W	0.5	SSL width
S	4	Length of SSL legs
T	0.1	Copper thickness
N	0.5	Substrate thickness

The SSL-FSS comprises narrow copper elements forming split square loops, imprinted on a single-layer dielectric, low-loss Rogers 4003C having εr = 3.55 and tan δ = 0.0027. The unit cell can be repeated indefinitely with a given periodicity that can be determined by adjusting the dielectric substrate size. Table 1 shows the parameters of the split square loop FSS.

3. SIMULATION

3.1 Simulation results

Simulations were performed using Computer Simulation Technology (CST) Microwave Studio, a comprehensive software package for high-frequency electromagnetic analysis. The simulator employs hexahedral grids with unit cell boundary conditions, as illustrated in Figure 6. For simplicity, the FSS was simulated as an infinite structure using master/slave boundary condition to impose periodic symmetry on the cell's sides, thus ensuring the electromagnetic field repeats as if the matrix were infinite. Floquet ports were used to simulate infinite periodic matrices by modeling a single, unary cell. These ports act as an excitation source for planar waves, enabling the precise calculation of the transmission and reflection coefficients (S21, S11).

A 3 × 3 array configuration minimized edge diffraction effects while maintaining computational efficiency, exhibiting less than 0.5 dB deviation in S-parameters compared to larger arrays (5 × 5). A 3 × 3 matrix is sufficient for modeling performance in a simulation environment to reduce computation time without sacrificing accuracy [13]. The FSS frequency response (band-stop or band-pass) depends on the element shape and type [25]. Figure 7 demonstrates that the split square loop FSS with s = 0 functions as a band-stop filter for varying gr values to understand the behavior of the single band before moving to the dual band. Here, the operating frequency is the resonant frequency (fr).

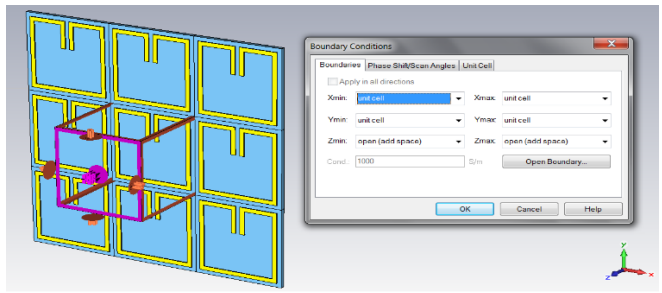

Figure 6. Computer Simulation Technology (CST) simulation setup with unit cell boundary conditions

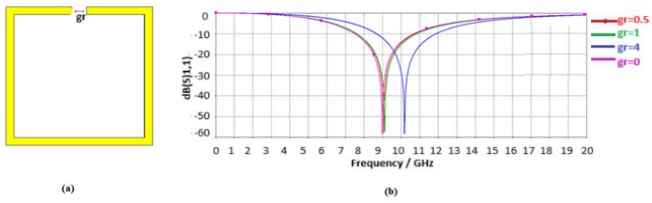

Figure 7. (a) Split Square Loop Frequency-Selective Surface (SSL-FSS) with length of SSL legs (s = 0), (b) The effect of varying the Length of gap (gr) between the SSL sides

Signals at frequencies lower or higher than fr are

transmitted by the structure's surface, but it also reflects signals at this frequency. In theory, bandwidth (BW) is determined by the difference between lower and upper frequencies at an S-parameter of -10 dB divided by the resonant frequency [26]. Table 2 lists the parameters of SSL FSS as the length of the ring gap (gr).

Table 2. Parameters of Split Square Loop Frequency-Selective Surface (SSL-FSS) with varying the Length of ring gap (gr)

gr (Length of Gap-mm)	fr (the Resonant Frequency (GHz))	Bandwidth
0	9	36.716%
0.5	9.07	36.069%
1	9.12	35.71%
4	10.156	32.65%

Figure 8 depicts the transmission response dependence on the length of the legs of the SSL element length (s) (all the parameters are unchanged). Variations in leg length (s) directly alter resonant frequencies, inducing dual-band behavior when s > 0. Increase of the length of legs(s) of SSL-FSS leads to decrease resonant frequency, but when (s > 0) there are two resonant frequency appear and meanwhile the bandwidth becomes narrower as illustrate in Table 3.

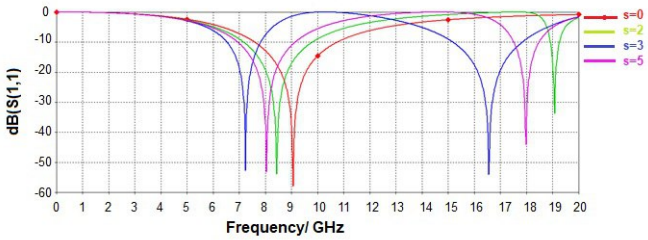

Figure 8. The effect of varying the length of the legs (s) of Split Square Loop Frequency-Selective Surface (SSL-FSS)

Table 3. Parameters of Split Square Loop Frequency-Selective Surface (SSL-FSS) with varying the length of the legs (s)

s (Length of Gap-mm)	fr1 (GHz)	fr2 (GHz)	Bandwidth
0	9.06	0	35.198%
2	8.443	19.08	31.781%
3	8	18	26.545%
5	7.22	16.26	17.184%

Figure 9 depicts the variation in resonant frequency caused by a change in copper width. Except for the element width, all of the parameters remain unchanged. The resonant frequency rises proportionally to the width. The resonant frequency increases as the width increases. Meanwhile, as shown in Table 4, the bandwidth increases.

Table 4. Parameters of Split Square Loop Frequency-Selective Surface (SSL-FSS) with varying the width of the SSL (w)

w (Width of the SSL) mm	fr1 (GHz)	fr2 (GHz)	Bandwidth
0.5	15.4	0	27.52%
1	9.512	0	31.578%
2	8	18	44.593%

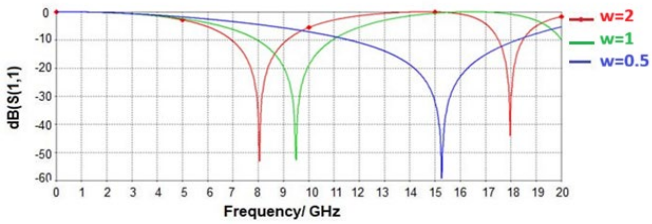

Figure 9. The impact of changing the copper width

Figure 10 depicts the variation in resonant frequency caused by changes in substrate thickness (n). As the thickness of the substrate increases, the resonant frequency and bandwidth decrease slightly as shown in Table 5.

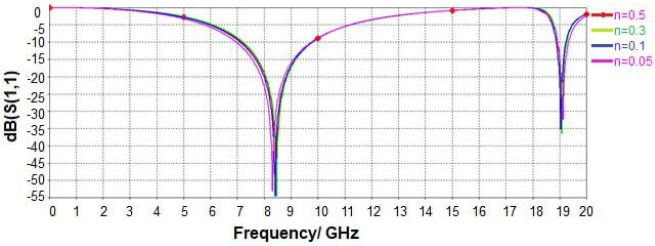

Figure 10. The impact on modifying the thickness of the substrate

Table 5. Parameters of Split Square Loop Frequency-Selective Surface (SSL-FSS) with varying the substrate thickness (n)

n (Substrate Thickness) mm	fr1 (GHz)	fr2 (GHz)	Bandwidth
0.05	8.3	19.12	33.768%
0.1	8.46	19.12	33.95%
0.3	8.46	19.12	33.95%
0.5	8.46	19.12	33.95%

3.2 Analysis for dual-band design

1. Gap Length (gr): Increasing g_r raises the first resonant frequency (fr1) but narrows bandwidth due to reduced capacitive coupling ($fr \propto 1/\sqrt{LC}$) [3, 5]. For dual-band operation, (gr) should be moderate to balance resonances between the two bands. Optimal value (gr = 0.5 mm) balances dual-band performance.

2. Copper Width (w): Increasing (w) increases the resonant frequency (fr1), bandwidth, and supports the second resonance needed for dual-band operation. A higher (w) value facilitates the second resonance appearance. Thicker substrates increase the effective permittivity ($\varepsilon_e$ff), which lowers ($fr \propto 1/\sqrt{\varepsilon_e}$ff) and reduces bandwidth due to higher dielectric loss [27]. Preferred (w = 2 mm), because it is permitting broader bandwidth and can be operated in dual-band mode.

3. Substrate Thickness (n): Thickness of substrates decreases resonant frequencies and bandwidth [28]. Both frequency and bandwidth are favored with thin substrates (n = 0.05 mm).

A small increase in (n) decreases resonant frequencies and decreases bandwidth. To operate in dual band mode, thinner substrates are better in order to retain the higher frequency bands and bandwidth [29, 30]. Value (n = 0.05 mm) recommended because it supports a higher resonant frequency.

4. Leg Length (s): As s increases there is a second resonance frequency (fr2). The extra inductance (s) of legs induces a second LC resonance. The structure also acts like two resonators at s = 0 that are coupled to each other (fr1 loop, fr2 leg-dominated path) [8, 31]. As presented in Table 3, with a 2-band mode, with fr1 = 8 GHz and fr2 = 18 GHz, recommended value (s = 3 mm).

Contemporary communication systems demand a high capacity and multifrequency band (dual-band) but existing designs are affected by either sophisticated design or poor performance.

This paper presents an SSL design that has been optimally refined by analyzing four main factors (g_r, s, w, n). An "independent control mechanism" uses legs of length (s) to bring about innovation. At s > 0, the architecture becomes a pair of resonators which are coupled together:

◦ The core loop controls the first band (fr1 8 GHz).

◦ The second band (fr2 18 GHz) is due to the extra inductance of the legs (s). This enables the second frequency to be controlled and restricted without greatly impacting the first frequency, thereby being able to overcome the "control deficit."

According to Table 6, this study is outstanding in three ways together:

• **Bandwidth:** The design had a bandwidth of 44% higher than expected in the table in previous works, with similar designs [16, 18, 21] having a range between 20% and 30%.

• **Compactness:** The design achieves high performance using a single passive layer. Designs offering wider bandwidth [12] are multi-layered, and those offering flexibility [17] lack dual-band functionality.

• **Control:** The experiment showed that besides increasing the frequency, the width of the copper (w), is also the secret to a huge increase in bandwidth.

Consequently, this novelty of the research is not just a parametric study but the discovery of the best engineering combination that enables a simple structure (SSL-FSS) to attain a tremendous bandwidth (44%) and the capacity to modulate the frequencies of the two (X and Ku) independently, which previously had to be done with complex or active structures.

Table 6. Comparison to the previous design

Ref.	Key Design Features	Operation Bands / Application	Resonant Freq. (GHz)	BW (%)	Polarization / Angular Stability	Type of Design	Advantages/ Limitations
[15]	Miniaturized; Bending technique	Radome / Angular-stable applications	2.4	Narrow	Angular stability up to 60°	Single-layer FSS	Small unit size (0.048λ) but limited bandwidth
[16]	Miniaturized Jerusalem cross	Ku-Band (Radar)	12-18	25-30%	Single-band focus	Jerusalem Cross FSS	Robust but bulky for mobile applications
[17]	Graphene-based, dynamic tuning	Cognitive Radio	6-12	35-45%	Polarization-agnostic	Reconfigurable FSS	Compact but lacks dual-band operation
[18]	Compact unit cells; low freq. ratio	X/Ku-Band (Wireless, IoT)	9, 15	~30%	Dual-Polarization	Compact Dual-Band FSS	Reconfigurable but high fabrication cost
[21]	U-shaped resonators with ground vias	Wireless communication / Dual-band applications	3.5, 5.5	6.2%-8.5%	One band insensitive, one band selective / Stable up to 45°	Dual-band FSS	Independent polarization control but moderate bandwidth
[24]	Graphene-based; voltage-controlled reconfigurability	Cognitive radio / Dynamic spectrum management	2.1-5.2 (tunable)	10-15 (tunable)	Polarization-insensitive / Stable up to 50°	Active Reconfigurable FSS	Continuous frequency tuning but high loss and complex fabrication
This Work	Split Square Loop (SSL)	X/Ku-Band (Radar, Satellite)	8, 18	36-44%	Polarization-insensitive	Dual-Band SSL-FSS	Balanced high bandwidth & compactness; passive design

Note: FSS: Frequency Selective Surface; SSL: Split Square Loop Frequency; SSL-FSS: Split Square Loop Frequency-Selective Surface

4. CONCLUSIONS

This paper has examined the dual-band performance of an SSL-FSS via simulations and parametric analysis. The findings prove that resonant frequencies and bandwidth strongly depend on varying the critical parameters: gap length (g_r), leg length (s), copper width (w) and substrate thickness (n). To begin with, it generally improves the resonant frequency but decreases the bandwidth with the best balance at g_r = 0.5 mm. Second, adding a second resonance, which is a second s, allows dual-band behavior. It is verified that parametric studies indicate that dual-band operation critically depends on leg length (s). At s = 3 mm resonant frequencies of 8 GHz (X-band) and 18 GHz (Ku-band) are obtained, and bandwidths of up to 44% are obtained by target applications. Third, broader copper strips (w = 2 mm) are associated with an increase of bandwidth and the possibility to use two bands. Finally, thinner substrates.

The resonant frequencies and bandwidths of (n = 0.05 mm) are larger and maintain a high resonant frequency. The suggested design can be used in X- and Ku-band applications. Future work will:

(1) Design and develop a prototype and test it on Rogers 4003C substrate and VNA.

(2) applying machine learning and artificial intelligence ML/AI to cope with the complexity of design of advanced reconfigurable FSS. This will make the field shift to the manual analysis of the parameters to the intelligent predictive

design frameworks.

REFERENCES

[1] Tong, X.C. (2017). Metamaterials inspired frequency selective surfaces. Functional Metamaterials and Metadevices, pp. 155-171. https://doi.org/10.1007/978-3-319-66044-8_8

[2] Sanz-Izquierdo, B., Parker, E.A., Robertson, J.B., Batchelor, J.C. (2009). Singly and dual polarized convoluted frequency selective structures. IEEE Transactions on Antennas and Propagation, 58(3): 690-696. https://doi.org/10.1109/TAP.2009.2039321

[3] Singh, G. (2012). A simple synthesis technique of single-square-loop frequency selective surface. Progress in Electromagnetics Research B, 45(45): 165-185. https://doi.org/10.2528/PIERB12090104

[4] Somwanshi, D.K., Bansal, P. (2024). Design and analysis of dual band frequency selective surface. In Radar and RF Front End System Designs for Wireless Systems, pp. 218-244. https://doi.org/10.4018/979-8-3693-0916-2.ch009

[5] Shittu, I., Abou-Khousa, M., Viegas, J., Hernandez-Figueroa, H.E., Elfadel, I.M. (2025). Radar cross section reduction metamaterials: A review of principles, design methods, and applications beyond. IEEE Aerospace and Electronic Systems Magazine, https://doi.org/10.1109/MAES.2025.3526134

[6] Idrees, M., He, Y., Ullah, S., Wong, S.W. (2024). A dual-band polarization-insensitive frequency selective surface for electromagnetic shielding applications. Sensors, 24(11): 3333. https://doi.org/10.3390/s24113333

[7] Kanagasabai, M., Ramadoss, S., Viswanathan, L., Mohammed, G.N.A., Shanmuganathan, S., Palaniswamy, S.K. (2024). A novel ultra-miniaturized angularly stable frequency selective surface for l-band shielding applications. International Journal of Antennas and Propagation, 2024(1): 8777541. https://doi.org/10.1155/2024/8777541

[8] Munk, B.A. (2005). Frequency Selective Surfaces: Theory and Design. John Wiley & Sons.

[9] HAMID, F.S. (2015). Optimized ELM with CNN depending on DSC for brain lesion segmentation in ISLES 2015. Middle East Journal of Scientific Research, 8(4): 1-13. https://doi.org/10.63085/mejsp/856420

[10] Jasim, M.B., Sayidmarie, K.H. (2022). Planar absorbing FSS unit cells for radar cross-section reduction. In 2022 International Conference on Innovation and Intelligence for Informatics, Computing, and Technologies (3ICT), Sakheer, Bahrain, pp. 476-480. https://doi.org/10.1109/3ICT56508.2022.9990893

[11] Hong, J.S.G., Lancaster, M.J. (2004). Microstrip Filters For RF/Microwave Applications. John Wiley & Sons.

[12] Fallahi, A. (2010). Optimal design of planar metamaterials. Ph.D. thesis, University of Tehran, 2010.

[13] Anwar, R.S., Mao, L., Ning, H. (2018). Frequency selective surfaces: A review. Applied Sciences, 8(9): 1689. https://doi.org/10.3390/app8091689

[14] Mittra, R., Chan, C.H., Cwik, T. (1988). Techniques for analyzing frequency selective surfaces-A review. Proceedings of the IEEE, 76(12): 1593-1615. https://doi.org/10.1109/5.16352

[15] Che, Y.X., Wu, S.J., Li, M., Ban, Y.L. (2025). Research progress on FSS stealth radome. Electronics, 14(6): 1132. https://doi.org/10.3390/electronics14061132

[16] Chen, X., Tan, J., Kang, L., Tang, F., Zhao, M., Kato, N. (2024). Frequency selective surface toward 6G communication systems: A contemporary survey. IEEE Communications Surveys & Tutorials, 26(3): 1635-1675. https://doi.org/10.1109/COMST.2024.3369250

[17] Kanth, V.K., Raghavan, S. (2019). EM design and analysis of frequency selective surface based on substrate-integrated waveguide technology for airborne radome application. IEEE Transactions on Microwave Theory and Techniques, 67(5): 1727-1739. https://doi.org/10.1109/TMTT.2019.2905196

[18] Kapoor, A., Mishra, R., Kumar, P. (2021). Slotted wideband frequency selective reflectors for sub-6 GHz 5G devices. In 2021 International Conference on Computing, Communication, and Intelligent Systems (ICCCIS), Greater Noida, India, pp. 786-791. https://doi.org/10.1109/ICCCIS51004.2021.9397157

[19] Sarika, M.R.T., Ronnow, D. (2018). A wideband frequency selective surface reflector for 4G/X-band/Ku-band. Progress in Electromagnetics Research C, 81: 151-159. http://doi.org/10.2528/PIERC18010908

[20] Ramadoss, S., Kanagasabai, M., Mohammed, G.N.A. (2022). A novel miniaturized band-stop frequency selective surface with ultra-wideband characteristics. Radio Science, 57(11): 1-12. http://doi.org/10.1029/2022RS007439

[21] Xue, Z., Zhong, S., Ma, Y. (2021). Graphene-FSS hybrid absorptive structure with amplitude/frequency dual-modulated passband. IEEE Antennas and Wireless Propagation Letters, 20(9): 1711-1715. http://doi.org/10.1109/LAWP.2021.3094835

[22] Cheng, T., Jia, Z., Hong, T., Jiang, W., Gong, S. (2020). Dual-band frequency selective surface with compact dimension and low frequency ratio. IEEE Access, 8: 185399-185404. https://doi.org/10.1109/ACCESS.2020.3030131

[23] Ma, Y.H., Wang, D.W., Yu, Y., Zhao, W.S. (2022). Design of dual-band frequency-selective surfaces with independent tunability. IEEE Transactions on Antennas and Propagation, 70(12): 12381-12386. https://doi.org/10.1109/TAP.2022.3209263

[24] Qin, T., Huang, C., Cai, Y., Lin, X. (2023). Dual-band frequency selective surface with different polarization selectivity for wireless communication application. Sensors, 23(9): 4264. https://doi.org/10.3390/s23094264

[25] Moniruzzaman, M., Larguech, S., Mobarak, M., et al. (2025). Dual band polarization insensitive metamaterial absorber for EMI shielding from GSM and 5G communication systems. Scientific Reports, 15: 12292. https://doi.org/10.1038/s41598-025-96507-4

[26] HAMID, F.S., Jasim, T.A., Alsultan, R.G. (2026). Vehicular-to-Everything (V2X) Communication using 5G NR for autonomous vehicles. Journal of Engineering, 2026(1): 8643947. https://doi.org/10.1155/je/8643947

[27] Hamid, F.S., Jarjes, M.K., Hussain, M.K. (2020). Simulating of OFDM systems for noise cancellation in the LTE application. International Journal of Enhanced

Research in Science, Technology & Engineering, 8(6).
[28] Hamid, F.S. (2013). The difference between IEEE 802.16/WiMAX and IEEE 802.11/Wi-Fi networks for Telemedicine. Applications. International Journal of Recent Technology and Engineering (IJRTE), 2(5): 2277-3878.
[29] Alsultan, R.G., Yetkin, G.Ö. (2018). Mutual couplingsuppression of closely spaced microstrip antennas by ladder-shaped conducting wall. International Journal of Communication Systems, 31(17): e3798. https://doi.org/10.1002/dac.3798.
[30] Ramadhan, S.K., Yousif, F.A., Hamid, F.S. (2025). Enhancing user experience with hand gesture volume control: Overcoming challenges of camera distance. Cybernetics and Physics, 14(4): 375-382. doi.org/10.35470/2226-4116-2025-14-4-375-382.
[31] Li, W., Li, Y. (2017). A high selectivity, miniaturized, low profile dual-band bandpass FSS with a controllable transmission zero. International Journal of Antennas and Propagation, 2017(1): 7983567. https://doi.org/10.1155/2017/7983567